Sensors & Actuators: B. Chemical 417 (2024) 136077

Contents lists available at ScienceDirect

Sensors and Actuators: B. Chemical

journal homepage: www.elsevier.com/locate/snb

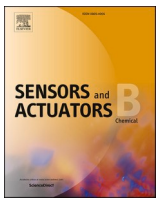

High-performance optical fiber differential urea sensing system for trace urea concentration detection with enhanced sensitivity using liquid crystals

Li Jin [a], Bowen Yang [a], Ze Xu [a], Wenwen Wang [a], Jizhou Wu [a,b], Dandan Sun [a,*], Jie Ma [a,b,**]

[a] School of Physics and Electronic Engineering, Shanxi University, Taiyuan 030006, China
[b] Collaborative Innovation Center of Extreme Optics, Shanxi University, Taiyuan 030006, China

ARTICLE INFO

Keywords:
Microfiber interferometer
Fiber Bragg grating
Differential demodulation
Liquid crystals
Urea detection

ABSTRACT

A compact optical fiber differential sensing system consisting of microfiber interferometer (MFI) functionalized urease combined with stearic acid (SA)-doped 4-cyano-4′-pentylbiphenyl (5CB) and two fiber Bragg gratings (FBGs) for urea detection has been proposed and experimentally demonstrated. The SA-doped 5CB plays an important role of sensing signal amplification in urease specific recognition of urea. The hydrolysis reaction between urea and urease at the microfiber surface causes the deprotonation and self-assembly of SA, which further induces the reorientation of 5CB from planar alignment to homeotropic alignment. This process can be captured and transduced into the macroscopic wavelength shift of the MFI and power difference of two FBGs in the differential sensing system. The experimental results show that the differential sensing system can effectively detect urea in artificial urine, where the sensitivity of MFI is 3.85 nm/mM with a detection limit of 0.03 mM and the power difference sensitivity of two FBGs is 15.05 dB/mM with a detection limit of 0.01 mM within low concentration range of 0.01–0.1 mM. Furthermore, the differential sensing system has good selectivity, affordability, and temperature self-compensation. Therefore, the differential sensing system can be used as a sensitive method for urea detection and has potential applications in human health detection.

1. Introduction

With the rapid development of the economy, a number of people are in a state of subhealth due to the change of environment and work pressure. In recent years, people's health awareness has been improving and human health testing and medical care have received increasing attention. Urea is the end product of protein metabolism in the human body, and is mainly excreted from the body in the form of urine through the kidneys [1]. Urea level in the human body can provide key information on kidney function and serve as a diagnostic basis for various kidney and liver diseases [2]. The urea content ranges in normal human urine from 0.155 to 0.39 M [3]. High urea levels indicate excessive protein intake, protein breakdown, and kidney damage [4]. In patients with severe diabetes, urea excreted by the kidneys is reduced, which indicates kidney problems or malnutrition [5]. Therefore, urea concentration detection is extremely crucial for human health.

On the basis of the previous studies, the methods used for urea detection and analysis mainly include high-performance liquid chromatography, the colorimetric method, chemical spectrophotometry, and the fluorescence method [6–10]. Although these methods can effectively and quantitatively detect urea concentration, they have some limitations that require the use of expensive measuring equipment, complex sample preprocessing processes, and fluorescent dyes to label biomolecules [11]. Therefore, it is extremely significant to find a simpler, low-cost, efficient, miniaturized, and highly sensitive method for urea concentration detection. Thus far, a lot of different optical fiber sensing methods for urea concentration detection have been reported. Priya Bhatia et al. fabricated a surface plasmon resonance (SPR) based optical fiber sensor for urea detection [12]. Guixian Zhu et al. developed a tapered coreless fiber sensor coated zeolite imidazole skeleton-8 (ZIF-8)/urease to detect urea concentration [13]. Liangliang Cheng et al. designed a highly sensitive fiber-optic SPR urea sensor based on ZIF-8/urease for urea concentration detection [14]. Sonika Sharma et al. reported a fiber optic SPR urea sensor based Ag/ITO/enzyme trapped gel layers to detect urea concentration [15]. These optical fiber sensing methods provide a basis for urea detection in terms of sensing structures. However, some of them have some disadvantages such as manufacturing complexity, high cost, and limited detection range. Microfiber sensors as

* Corresponding author.
** Corresponding author at: School of Physics and Electronic Engineering, Shanxi University, Taiyuan 030006, China.
E-mail addresses: sundd@sxu.edu.cn (D. Sun), mj@sxu.edu.cn (J. Ma).

https://doi.org/10.1016/j.snb.2024.136077
Received 4 December 2023; Received in revised form 29 May 2024; Accepted 3 June 2024
Available online 7 June 2024

a new sensing technology have an irreplaceable advantage in biomedicine due to their resistance to electromagnetic interference, miniaturization, corrosion resistance, biocompatibility, and remote sensing capability. Numerous studies have reported the use of microfiber for biosensing. Baiou Guan et al. developed an interface sensitized optical microfiber biosensor to detect neurotransmitter γ-amino-butyric acid and cellular cytochrome [16]. Yang Ran et al. fabricated an interstitial optical fiber needles for cancer sensing and therapy [17]. Hou Change et al. developed a tapered microfiber Mach-Zehnder interferometer (MZI) biosensor for sensitive Staphylococcus aureus detection [18].

Liquid crystals (LC), a special sensing material with birefringent property, have been widely applied in biomolecule detection, such as cholesterol, lipase, phospholipase, and penicillinase [19–22]. The orientation of LC is ultrasensitive to external stimuli at the surface, which can be amplified and transduced into optical signals to detect by using spectrum, such as transmission spectrum, reflection spectrum, and lasing spectrum [23–25]. At present, several studies that combine 4-cyano-4′-pentylbiphenyl (5CB) with optical fiber sensors are reported. Jianyang Hu et al. fabricated a tapered photonic crystal fiber sensor coated with penicillin G based 4′-pentyl-biphenyl-4-carboxylic acid (PBA)-doped 5CB to detect the penicillinase concentration [22]. Jieyuan Tang et al. achieved phospholipase concentration detection by using an alkoxysilane-modified side-polished fiber coated with 5CB and self-assembled phospholipid [21]. Stearic acid (SA), an amphiphilic saturated fatty acid molecule with a long hydrophobic chain tail and a hydrophilic head group, has structural properties similar to those of PBA, and the carboxyl functional group in its structure is very sensitive to the pH in the solution [26–28]. Therefore, the SA-doped 5CB is selected as the sensitive material to achieve the optical signal amplification.

In this research, in order to optimize the demodulation method of the wavelength demodulation based microfiber interferometer (MFI) and to reduce temperature cross-sensitivity, we cascaded the fiber Bragg gratings (FBGs) with the MFI to form an optical fiber differential sensing system. FBG, one of the most reliable and commercially available optical fiber sensors, supports high resolution interrogation and multiplexing [29]. Cheng Zhang et al. designed an intensity-modulated refractive index (RI) sensor with antilight source fluctuation based on a no-core fiber filter and two FBGs [30]. Stephanie Hui Kit Yap et al. achieved the lead ion detection by an advanced hang-held sensor based microfiber and two FBGs [31]. Therefore, an optical fiber differential sensing system consisting of MFI functionalized urease combined with SA-doped 5CB and two FBGs is proposed for urea concentration detection in both phosphate buffer solution (PBS) and artificial urine. The sensing mechanism of the sensing system is based on the RI measurement, where the RI sensitivity of the MFI is 1732.24 nm/RIU and the power difference sensitivity of two FBGs is 8532.49 dB/RIU. The hydrolysis of urea by urease produces hydroxide ions, bicarbonate ions, and ammonium ions resulting in an increase in pH, which triggers the realignment of 5CB contributed the deprotonation and self-assembly of SA at the surface of the MFI. This process not only alters the RI of 5CB, but also further induces the wavelength shift of the microfiber interferometer and the change of two FBGs power difference. The differential sensing system has obvious response to urea concentration in PBS, the sensitivity of MFI is 17.29 nm/mM with a detection limit of 0.007 mM, and the power difference sensitivity of two FBGs is 81.83 dB/mM with a detection limit of 0.002 mM. Moreover, in the tests of artificial urine, the sensitivity of the MFI is 3.85 nm/mM with a detection limit of 0.03 mM and the power difference sensitivity of two FBGs is 15.05 dB/mM with a detection limit of 0.01 mM. The proposed sensing system optimizes demodulation method and has a low detection limit for urea detection in artificial urine, which is expected to be used for the urea detection in human urine.

2. Materials and methods

2.1. Reagents and instruments

All reagents and instruments are described in Section 1.1 of the Supplementary Material.

2.2. Experimental setup

The light that was emitted by an amplified spontaneous emission light source (ASE) with a wavelength range of 1528–1603 nm and an output power of 10.5 mW successively reached the MFI, fiber circulator1, FBG1, fiber circulator2, FBG2 and optical spectrum analyzer (OSA) (range 600–1700 nm), as shown in Fig. 1 (blue dashed box). The MFI was placed in a groove made of PolyLite™ PLA materials to allow the microfiber to immerse in solution. The FBG1 and FBG2 were fixed on two glass slides separately. Two optical power meters (OPM) were connected by the third port of optical fiber circulator to monitor the power variation of FBG1 and FBG2. Finally, the transmission spectrum was recorded by the OSA with a resolution of 0.03 nm.

2.3. Differential sensing system fabrication

The differential sensing system consisted of a MFI and two FBGs. Furthermore, the MFI was constructed from a photosensitive fiber heated by butane flame with a width of about 2 mm for 8 s and uniformly stretched by a movement controller with a stretching initial speed of 2 mm/s and a tapering distance of 18 mm. While tapering the photosensitive fiber, the heat source remained stationary, and two stepper motors moved simultaneously along both ends of the fiber at the same speed under precise computer control with an accuracy of 1 μm. In this way, the MFI was successfully fabricated by automation. During the experimental process, to avoid the effect of different flame temperatures on the MFI, we waited for the temperature of the flame gun to return to room temperature before conducting the next experiment. Finally, the diameter of the MFI was gradually reduced from 125 μm to about 10 μm. The microfiber included two conical transition regions with a length of 3 mm and a waist region with a length of 13 mm and a diameter of 10 μm, as shown in Fig. 1 (red dashed box). Fig. 1 (red dashed box, up) shows the real images of the parts of the microfiber obtained by the metallurgical microscopy. Two FBGs with different Bragg wavelengths were selected at two linear regions of the MFI. In Section 1.3 of the Supplementary Material, Fig. S1 and Table S1 discussed the RI sensitivity of MFIs with different structural parameters. As a result, considering the existence of trade-offs between the sensitivity of the microfiber and the diameter of the waist region as well as the stability of the operation, we chose the MFI with a waist region diameter of about 10 μm for the fabrication of the microfiber biosensing probe.

2.4. Preparation of the experimental solution

All experimental solution preparations are described in Section 1.2 of the Supplementary Material.

3. Results and discussion

3.1. Sensing principle

3.1.1. Principle of the differential sensing system

When light enters the waist region from the down taper region of the microfiber, a portion of the light propagates along the core and another portion of the light propagates along the transition region, resulting in multiple higher-order modes being excited by the fundamental mode due to core diameter mismatch. Besides, throughout the waist region, the fundamental core mode and cladding mode are transmitted simultaneously, where the HE_{11} mode and the HE_{12} mode are mainly

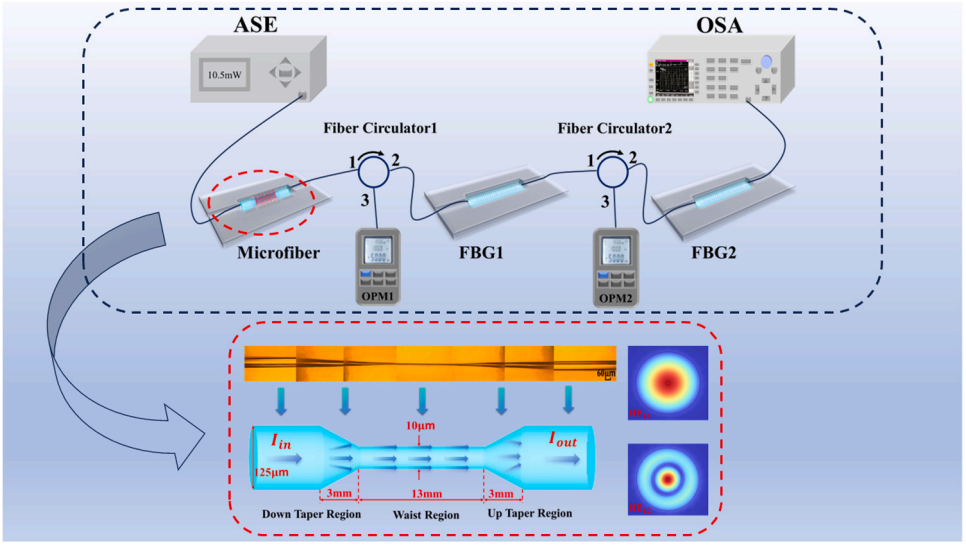

Fig. 1. Schematic diagram of the experimental setup and the structure of the MFI.

transmitted, as shown in Fig. 1 (red dashed box, right). Then, when the light propagates into the up taper region of the microfiber, the HE_{11} mode and HE_{12} mode are coupled. The RI sensitivity is an essential characterization of the MFI, which can be expressed as follows [32,33]:

$$\frac{d\lambda}{dn_{sm}} = \lambda \frac{1}{\Gamma}\left(\frac{1}{\Delta n_{eff}} \frac{d\Delta n_{eff}}{dn_{sm}}\right) \tag{1}$$

where n_{sm} is the RI of the surrounding medium (SRI) and λ is the wavelength of dip in transmission spectrum. Δn_{eff} is the effective RI difference between the core mode and cladding mode. $\Gamma = 1 - \frac{\lambda}{\Delta n_{eff}} \frac{d\Delta n_{eff}}{d\lambda}$ represents the dispersion factor and is negative, which characterizes the effect of the variation of the RI difference with wavelength [34]. $\frac{1}{\Delta n_{eff}} \frac{d\Delta n_{eff}}{dn_{sm}}$ is the dependence of the index difference on the SRI [35]. When the SRI increases, the RI exponents of the fundamental mode and the higher-order mode increase accordingly. Although the exponents of both the HE_{11} and HE_{12} modes increase as the SRI increases, the exponent of the HE_{12} mode increases larger than that of the HE_{11} mode. So, $\frac{1}{\Delta n_{eff}} \frac{d\Delta n_{eff}}{dn_{sm}}$ is a negative value. As a result, we conclude that $\frac{d\lambda}{dn_{sm}}$ is a positive value, which demonstrates that the wavelength of the microfiber will be redshifted with the SRI increase.

According to the reference [36], the Bragg wavelength of FBG is not affected by SRI. When the SRI increases, the wavelength of the microfiber will be redshifted while the Bragg wavelength of the FBG keeps unchanged. The Bragg wavelength of FBG is selected at two linear regions of the MFI. The slope of the two linear regions of the MFI is reversed. Thus the power of the two FBGs vary in opposite directions. The response of the power difference of two FBGs can be expressed as follows [30,31]:

$$\begin{aligned} \Delta P &= P_1 - P_2 \\ &= -\int_{-\infty}^{+\infty} S(\lambda) T_2(\lambda - \Delta\lambda) R_2 \delta(\lambda - \Delta\lambda) - \int_{-\infty}^{+\infty} S(\lambda) T_2(\lambda - \Delta\lambda) R_2 \delta(\lambda - \Delta\lambda) \\ &= R_1 S(\lambda_1) T_1(\lambda_1 - \Delta\lambda) - R_2 S(\lambda_2) T_2(\lambda_2 - \Delta\lambda) \end{aligned} \tag{2}$$

where ΔP is the power difference of the two FBGs, P_1 is the power of FBG1, P_2 is the power of FBG2, λ_1 is the Bragg wavelength of FBG1, λ_2 is the Bragg wavelength of FBG2, $\Delta\lambda$ is the wavelength shift of the MFI, $S(\lambda)$ is the power spectral density function of the light source, $T_1(\lambda)$ and $T_2(\lambda)$ are the initial transmission spectrum of the two linear regions of the microfiber, R_1 and R_2 are the reflective coefficients of the FBG1 and FBG2, $\delta(\lambda)$ is the unit pulse function, and $R_1\delta(\lambda - \lambda_1)$ and $R_2\delta(\lambda - \lambda_2)$ are the reflective spectrum functions of the FBG1 and FBG2. On the basis of the above analysis, the SRI can be measured by the power difference of two FBGs because of the wavelength shift of the MFI affected by the SRI.

3.1.2. Principle of urea detection

Before urea is detected, the MFI is sequentially modified by polydopamine (PDA), dimethyl octadecyl[3-trimethoxysilylpropyl] ammonium chloride (DMOAP), the SA-doped 5CB, glutaraldehyde (GA), and urease, as shown in Fig. 2(a, left). PDA is used to hydroxylate the surface of the MFI. DMOAP is used as the coupling agent molecule to fix the orientation of 5CB. SA-doped 5CB is used as the sensitive material. GA is acted as the cross-linking agent to immobilize urease. Urease is used as the recognized molecule to hydrolyze the urea. When urea is detected, it is hydrolyzed into hydroxide ions, bicarbonate ions, and ammonium ions, as shown in Fig. 2 (blue dashed box, middle) [25]. This process increases the pH of the solution, which causes the deprotonation and self-assembly of SA to form a monomolecular layer. This self-assembly process leads to the orientation transition of the 5CB molecules from planar to homeotropic alignment, as shown in Fig. 2(a, right), which not only alters the effective RI of 5CB molecules but also further induces the redshift of the MFI wavelength and the change of the power of two FBGs. Therefore, the hydrolysis of urea by urease can be detected by the differential sensing system. To verify the detection principle, experiments on the response of the differential sensing system to different pH values are performed. Fig. 2(b, left) shows the transmission spectrum of the differential sensing system for PBS in the pH range of 8.0–9.4. As the pH increases, the wavelength of the MFI redshifts, the intensity of FBG1 increases, and the intensity of FBG2 decreases. Fig. 2(b, right) shows the linear fitting of the MFI and two FBGs to pH from 8.0 to 9.4 in the differential sensing system. The wavelength of the MFI shifts by 1.79 nm and the two FBGs power difference changes by 5.24 dB, which indicates that the orientation change of 5CB can be characterized by the transmission spectrum of the differential sensing system.

3.2. RI and temperature performance of the differential sensing system

Fig. 3(a) shows the transmission spectrum of the differential sensing system, which consists of a cascade of three MFIs with identical structural parameters (waist region diameter of about 10 μm, waist region length of about 13 μm, and conical transition region length of 3 mm) and

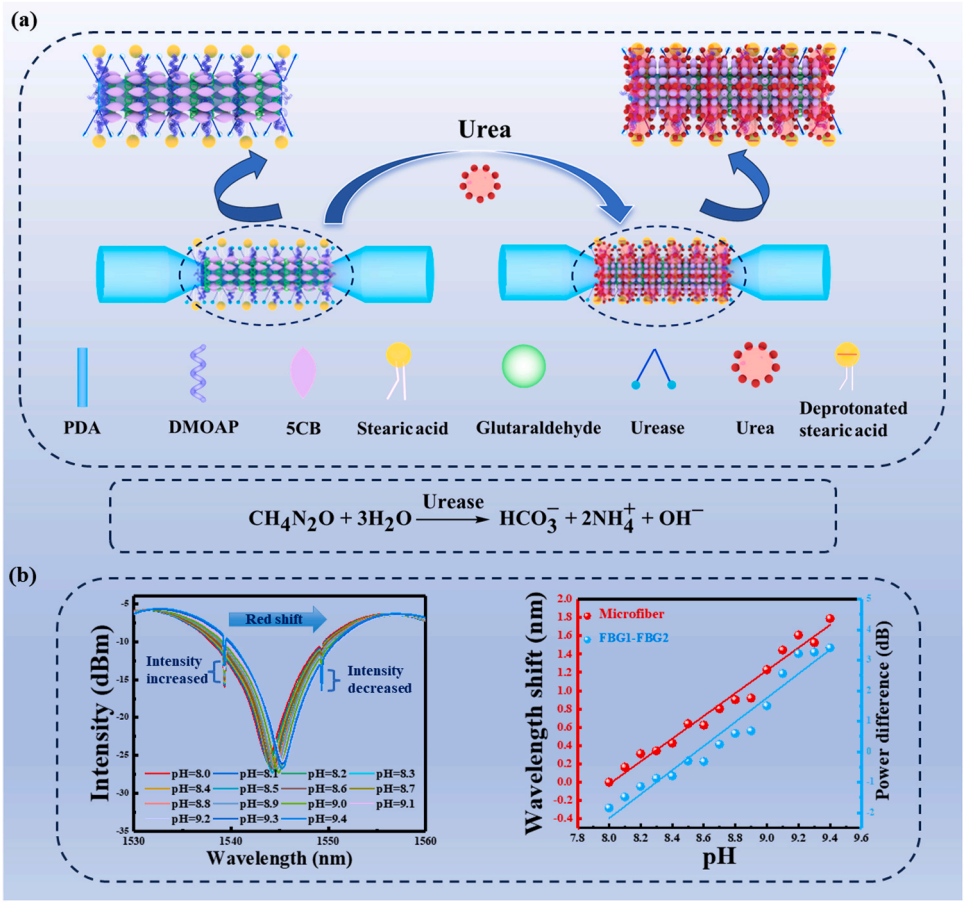

Fig. 2. (a) Schematic diagram of the urea detection principle. (b) (left): Transmission spectrum of the differential sensing system in the pH range from 8.0 to 9.4. (right): The linear fitting of the MFI and two FBGs in the differential sensing system in the pH range from 8.0 to 9.4.

two FBGs, respectively. The FBG1 and FBG2 are located in two linear regions of the dip of the MFI. The RI performance of the differential sensing system is measured by preparing the sodium chloride solution with different RI. The RI of the sodium chloride solution ranges from 1.3387 to 1.3415 obtained by digital refractometer. When the RI increases, the wavelength of MFI redshifts, the intensity of FBG1 increases, and the intensity of FBG2 decreases, as shown in Fig. 3(b). Fig. 3(c) further shows the intensity trends of two FBGs with the redshift of the MFI. Fig. 3(d) shows that the RI sensitivity of MFI is 1735.24 nm/RIU and the RI sensitivity of the two FBGs power difference is 8532.49 dB/RIU. Fig. 3(e) verifies the FBG response to temperature. When the temperature increases from 30 ℃ to 70 ℃ at 5 ℃ intervals, the Bragg wavelength of FBG1 redshifts with the temperature sensitivity of 0.0107 nm/℃ and the Bragg wavelength of FBG2 redshifts with the temperature sensitivity of 0.0105 nm/℃. Fig. 3(f) shows the temperature response of the differential sensing system after three experiments. The temperature sensitivity of MFI is −0.038 nm/℃, and the temperature sensitivity of the power difference of two FBGs is −0.33 dB/℃. As a result, the RI measurement errors caused by temperature for the MFI is about 2.19×10^{-5} RIU/℃ and the RI measurement errors caused by temperature for the power difference of two FBGs is about 3.86×10^{-5} RIU/℃, which further indicates that temperature has a small influence on the RI measurement of the differential sensing system.

3.3. Surface modification of the MFI sensing probe

In the differential sensing system, the functionalization of the MFI is a crucial step toward urea detection. As shown in Fig. 4, the modified process of the MFI sensing probe is as follows. Fig. 4(a) shows the bare MFI. Firstly, the bare microfiber is hydroxylated by immersing it in 2 mg/ml PDA solution for 40 min, as shown in Fig. 4(b). The treated MFI is rinsed with plenty of deionized water (DI) to remove the excess PDA. Next, the hydroxylated microfiber is silanized with 0.5 % v/v DMOAP solution for 10 min, as shown in Fig. 4(c). Then, the silanized MFI is rinsed with plenty of DI and dried for half an hour in air to remove the excess DMOAP and fix the orientation of the SA-doped 5CB, respectively. Subsequently, the 0.25 % v/v SA-doped 5CB is smeared on the surface of DMOAP modified microfiber within 3 min, as shown in Fig. 4(d). Then, the SA-doped 5CB smeared microfiber is modified with 1 % v/v GA solution for 40 min, as shown in Fig. 4(e). Furthermore, the modified microfiber is immersed into the DI to remove the excess GA. As shown in Fig. 4(f), the GA modified microfiber is immersed in the urease solution with a concentration of 0.01 g/ml for 40 min. Then, the MFI is immersed in the DI to remove the excess urease. Finally, the MFI sensing probe for urea detection is successfully fabricated. All experimental processes are conducted at room temperature.

3.4. Characterization of the MFI sensing probe for urea detection

Fourier transform infrared (FTIR) is used to characterize the successful attachment of individual functional films during the fabrication of the MFI sensing probe. Fig. 5(a) shows the FTIR spectrum of PDA, where the characteristic peaks in the range at 3500–3000 cm^{-1} are the N–H and O–H stretching vibrations [37]. The intense peak around 1756 cm^{-1} is attributed to the C=O of the quinone group [37]. The characteristic peaks of 1603.76 cm^{-1} and 1523.31 cm^{-1} are the C=C in the aromatic system and the C=N of the indole amine, respectively [37]. Another peak at 1314 cm^{-1} is the C–N stretching of the indole ring [37].

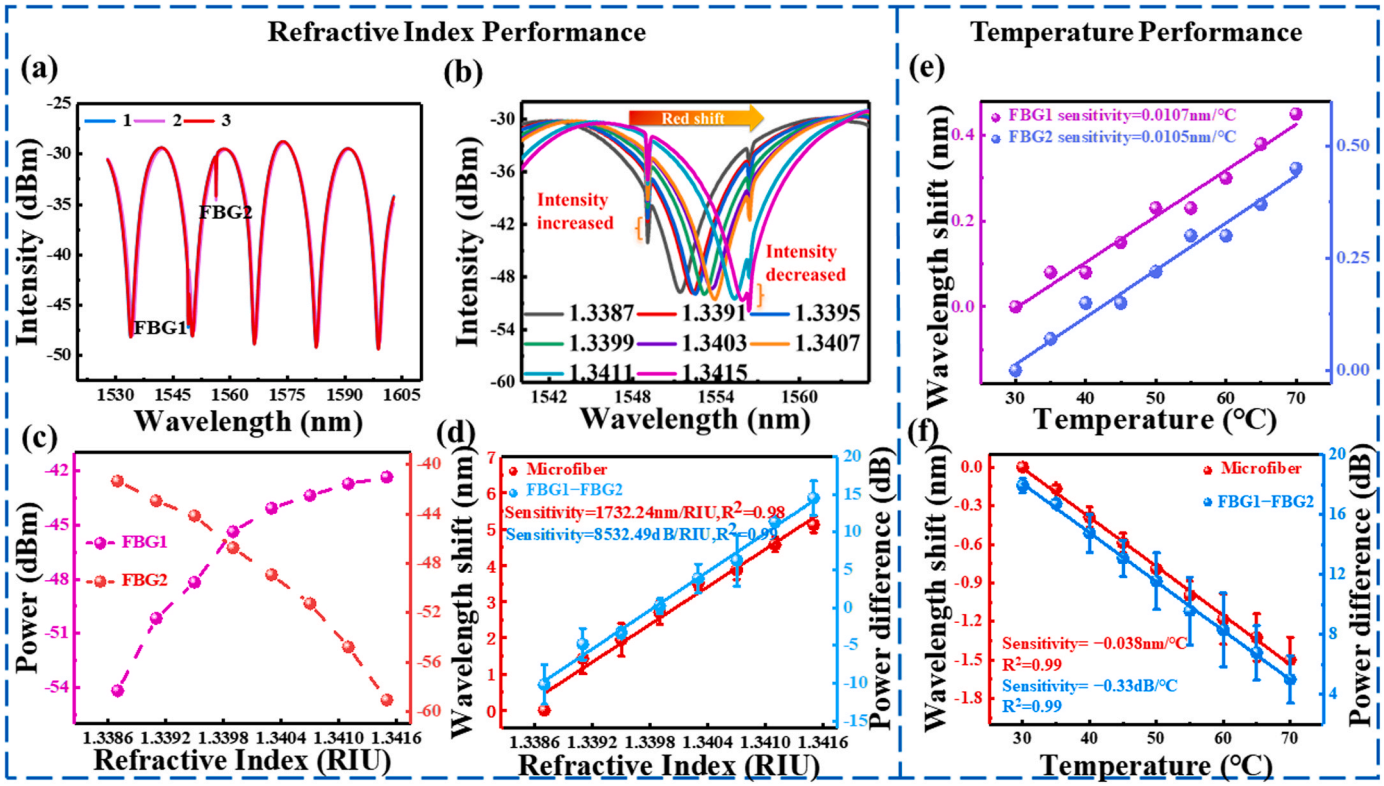

Fig. 3. Experimental results of the RI and temperature performance of the differential sensing system.

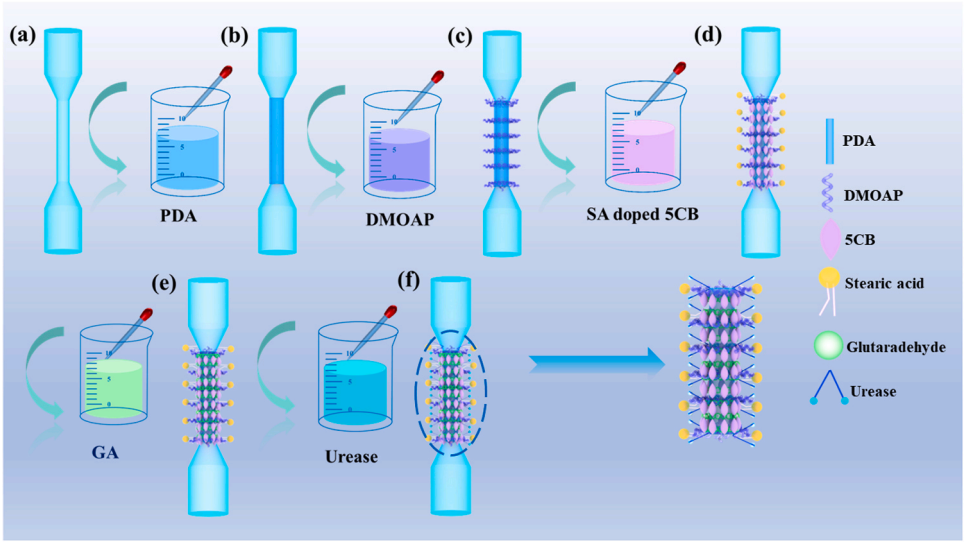

Fig. 4. Schematic diagram of the fabrication of the MFI sensing probe.

Therefore, the formation and chemical functionality of PDA on microfiber is demonstrated by the analysis of the above functional groups. Fig. 5(b) shows the FTIR spectrum of PDA combined with DMOAP, where the characteristic peaks at 2926 cm^{-1} and 2855 cm^{-1} are the CH_3 and CH_2 stretching of DMOAP [38,39]. The absorption peaks of 1284.02 cm^{-1} and 1202.66 cm^{-1} can be attributed to the stretching vibrations of the Si–C and C–O [39]. The absorption peak of 1244.66 cm^{-1} confirms the formation of the Si–O. The absorption peak of 1078.62 cm^{-1} presents the formation of the Si–O–Si bond, which demonstrates that the hydroxylated microfiber is silanated [38]. Fig. 5 (c) shows the FTIR spectrum of PDA/DMOAP/SA-doped 5CB. The absorption peak at 2250 cm^{-1} corresponds to the C≡N bond in 5CB [39, 40]. The absorption peak of 1720 cm^{-1} is the C=O stretching of the carboxylic group, which confirms the presence of SA [41,42]. The characteristic peaks at 2926 cm^{-1} and 2855 cm^{-1} is attenuated to 2917.14 cm^{-1} and 2852 cm^{-1}, which can be presumed that the 5CB is smeared by DMOAP [39]. Fig. 5(d) shows that the absorption peaks at 1657.53 cm^{-1} and 2917.91 cm^{-1} can be attributed to the –C=O stretching of the free aldehyde and the –CH stretching, which confirms the presence of GA [41]. The absorption peak of 1076.61 cm^{-1} presents the formation C–O–C bond, which indicates the successful attachment of GA to SA [43]. Fig. 5(e) shows that the absorption peak at 3222.32 cm^{-1} is the –NH stretching vibration due to the stretching of the cysteamine dihydrochloride of urease [44]. In addition, the other characteristic

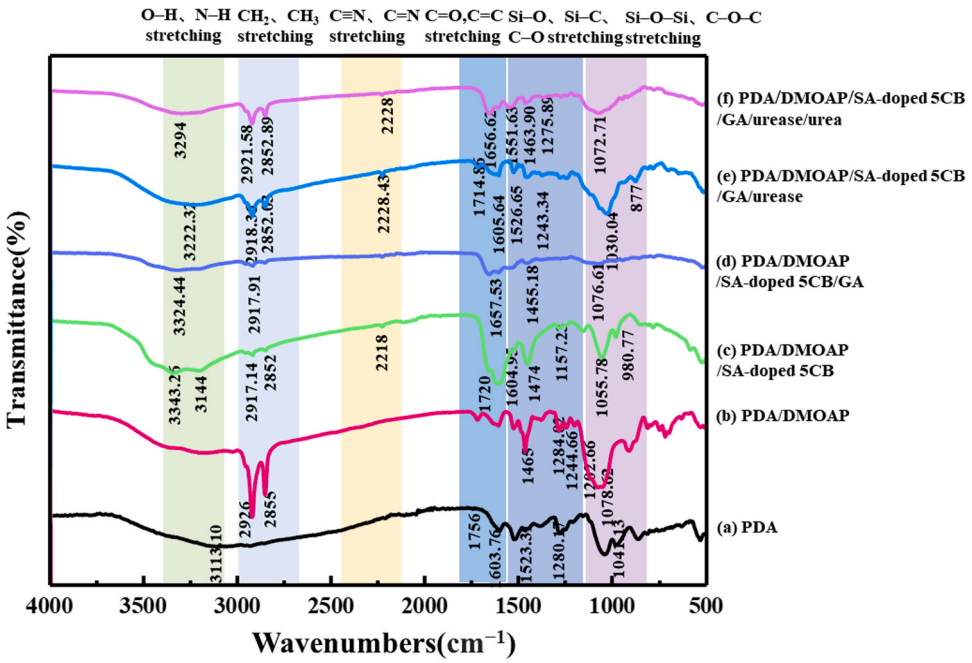

Fig. 5. Fourier transform infrared spectrum of (a) PDA. (b) PDA/DMOAP. (c) PDA/DMOAP/SA-doped 5CB. (d) PDA/DMOAP/SA-doped 5CB/GA. (e) PDA/DMOAP/SA-doped 5CB/GA/urease. (f) PDA/DMOAP/SA-doped 5CB/GA/urease/urea.

peaks of 1030.04 cm^{-1} and 877 cm^{-1} are the stretching of C–H and =C–H bending [44]. The absorption peak at 2228.43 cm^{-1} is the formation of the –C=N bond, which confirms the successful cross-linking of urease and GA[44]. Fig. 5(f) shows that the absorption peak of 1656.62 cm^{-1} is the C=O stretching vibration of the amide band of urea [43]. The characteristic peaks of 1551.63 cm^{-1}, 1463.90 cm^{-1}, and 1275.89 cm^{-1} represent the carbonate group stretching vibration, which indicates that the urea is hydrolyzed by urease [43].

3.5. Differential sensing system response during modification

3.5.1. Response of differential sensing system modified by PDA and DMOAP

According to the Section 3.3, the bare microfiber is immersed in the PDA solution. PDA grows in situ on the surface of the microfiber because of its strong adhesion properties. After 40 min of polymerization, a large number of hydroxyl groups are attached to the microfiber surface, making the microfiber hydrophilic. Fig. 6(a) shows the change of transmission spectrum with the polymerization time from 0 min to 40 min at 4 min intervals. The wavelength redshift of MFI is an average of 3.6 nm and the average power difference of two FBGs increases from −3.74 to 10.99 dB, as shown in Fig. 6(b). Then, the alkoxy groups in DMOAP bind to the hydroxyl groups on the surface of microfiber via covalent bond. Fig. 6(c) shows the response of the coated PDA MFI to DMOAP, where the wavelength redshift of MFI is an average of 0.43 nm and the average power difference of the two FBGs increases from 3.33 to 4.29 dB.

3.5.2. Response of the differential sensing system modified by SA-doped 5CB

After modifying by PDA and DMOAP, the MFI is immersed in the SA-doped 5CB solution. Orienting groups in DMOAP enable the SA-doped 5CB molecules to align planarly on the surface of MFI. Fig. 7(a) shows the transmission spectrum of the MFI immersed in SA-doped 5CB solution for 3 min. Fig. 7(b) is the fit to the wavelength shift and the power difference in one experiment. When the coating time exceeds 2 min, the wavelength shift and power difference of the differential sensing system remain essentially unchanged, which indicates that the orientation of

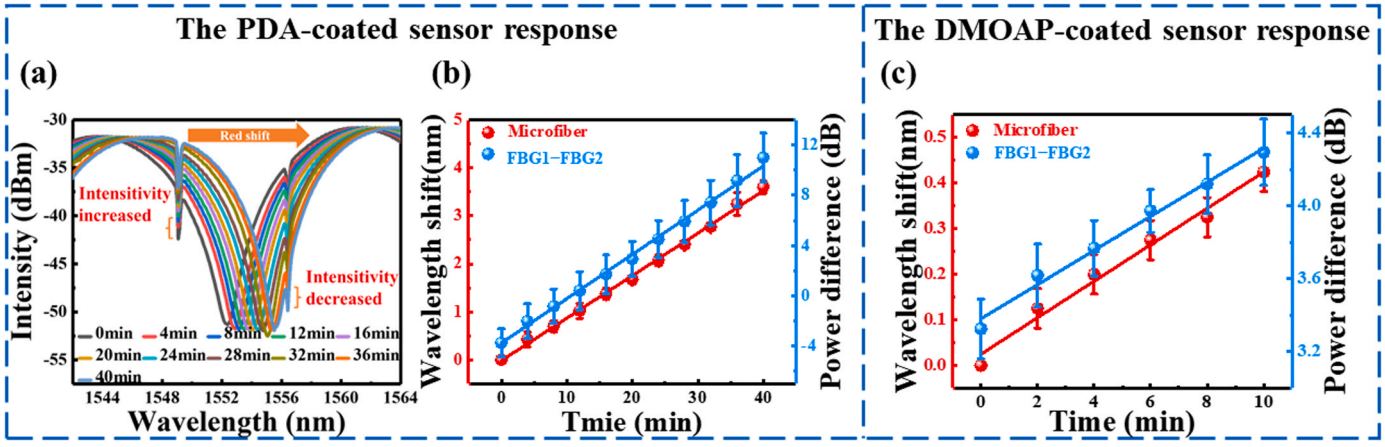

Fig. 6. (a) Local magnification of the transmission spectrum of the MFI in the PDA coating process. (b) Response of the differential sensing system to PDA. (c) Response of the differential sensing system to DMOAP.

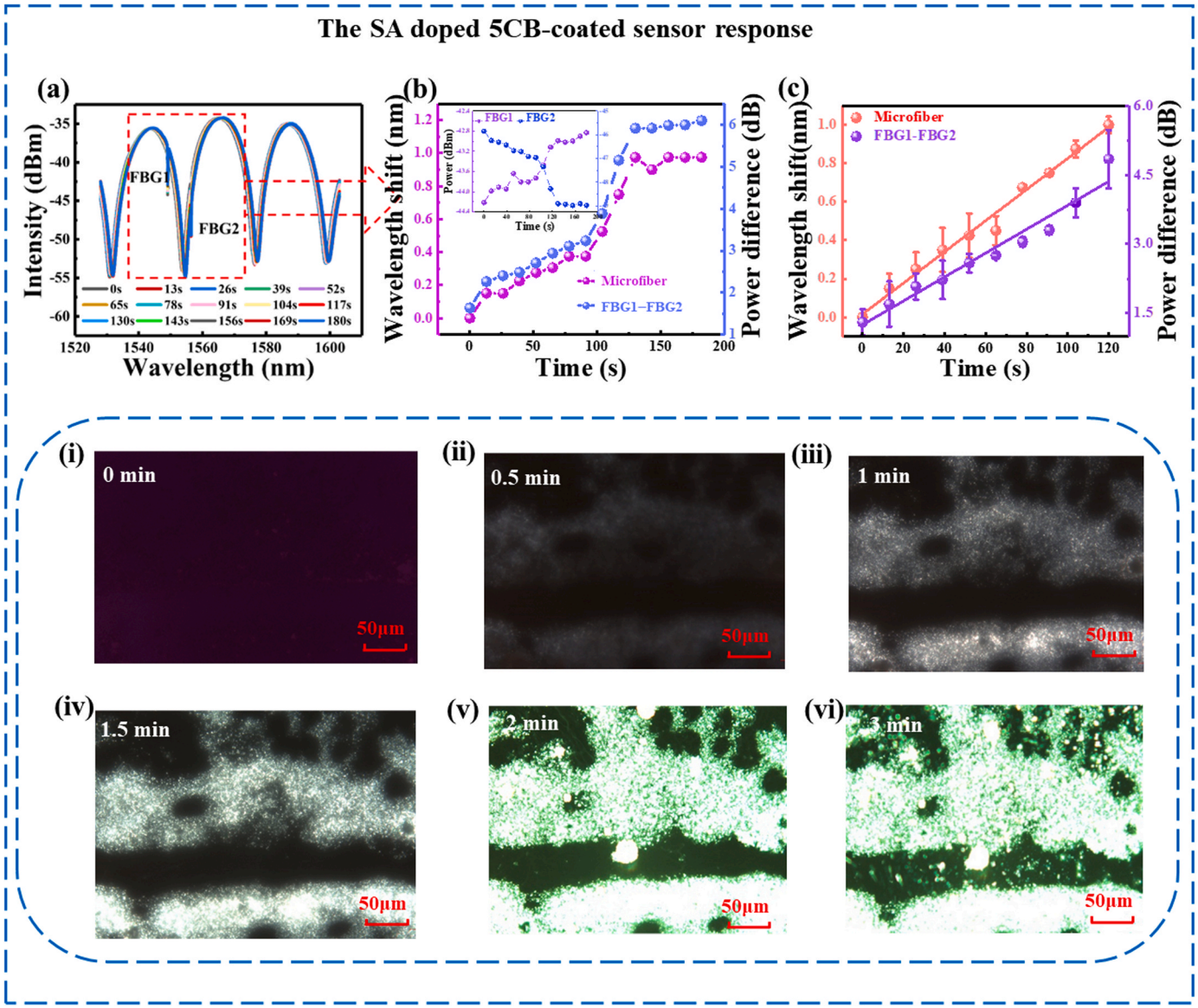

Fig. 7. (a) Transmission spectrum of the differential sensing system to SA-doped 5CB. (b) The MFI wavelength shift and two FBGs power difference change, the inset is the power change of FBG1 and FBG2. (c) Response of the differential sensing system to SA-doped 5CB. The inset is the polarize optical microscope (POM) images of SA-doped 5CB on the slide.

the SA-doped 5CB keeps in a stable state of planar alignment. Fig. 7(c) shows that within 2 min, the wavelength redshift of MFI is an average of 1 nm and the average power difference of two FBGs increases from 1.3 to 4.84 dB. To characterize the planar alignment of 5CB molecules on the MFI, we perform the same modification on the slide and observe the light and dark change of 5CB appearance under POM. The inset of Fig. 7 shows the corresponding POM images of the appearance of 5CB within 3 min. Fig. 7((i)) shows that a dark appearance can be observed under the POM, when the mixing solution of SA and 5CB is added dropwise to the slide coated DMOAP. Fig. 7(ii) shows the bright spots begin appearing after 0.5 min. Fig. 7(iii) shows that the number of bright spots displayed gradually increases after 1 min. Fig. 7(iv) shows that the bright spots gradually become brighter and larger after 1.5 min. Fig. 7 (v)–(vi) show that the bright spots become larger and larger and maintain a steady state of brightness after 2 min. The main reason for the above changes is the SA dissolving in 5CB and forming reverse micelles, which disturbs the orientation of the 5CB [45].

3.5.3. *Response of the differential sensing system modified by GA and urease*

After modifying by SA-doped 5CB, the MFI is modified by the GA and urease, respectively. When the MFI is immersed in the GA solution, the aldehyde group of GA combines with the carboxyl group of SA to form a covalent bond. Fig. 8(a) shows that the wavelength redshift of MFI is 0.68 nm and the power difference of the two FBGs increases from −10.5 to −8.5 dB. When the MFI modified GA is immersed in the urease solution, the aldehyde group of GA reacts with amino group of urease to form the imine bond. As shown in Fig. 8(b), when the coating time exceeds 40 min, the wavelength shift and power difference of the differential sensing system remain essentially unchanged. Therefore, 40 min is selected as the optimal coating time. The inset in Fig. 8(b) is the power change of the FBG1 and FBG2. Fig. 8(c) shows that the wavelength redshift of MFI is an average of 0.85 nm and the average power difference of the two FBGs increases from −12.52 to −8.15 dB.

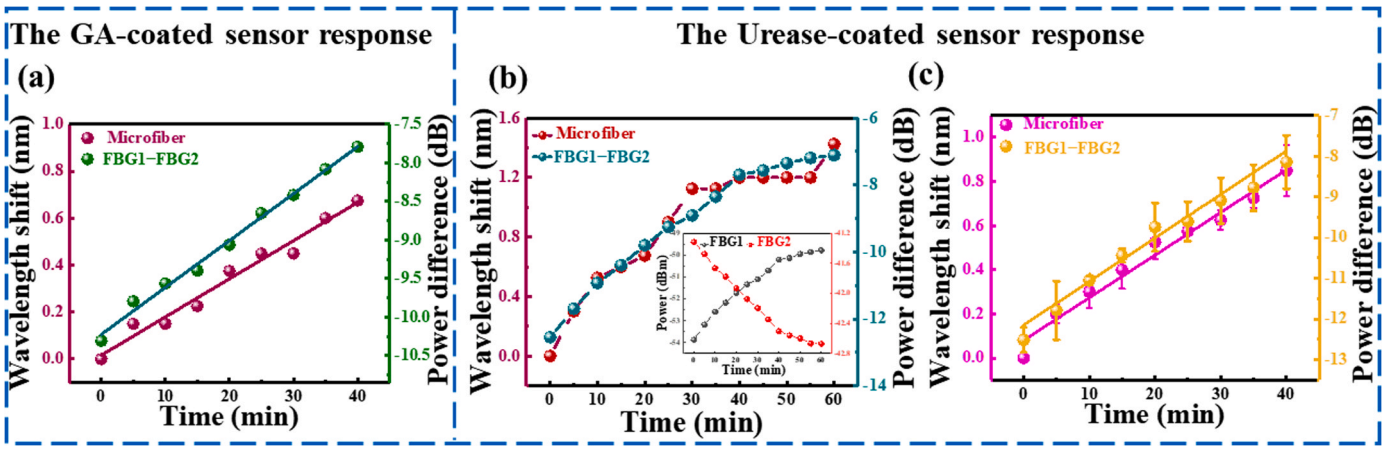

Fig. 8. (a) Response of the differential sensing system to GA. (b) The wavelength shift of the MFI and the change of two FBGs power difference to urease, the inset is the power change of FBG1 and FBG2. (c) Response of the differential sensing system to urease.

3.6. Urea detection in PBS

In this experiment, based on the urea detection principle described in Section 3.1.2, the hydrolysis reaction between urea and urease causes the deprotonation and self-assembly of SA and the reorientation of the 5CB from planar alignment to homeotropic alignment, which can be transduced into the MFI sensing probe wavelength shift and the change of two FBGs power difference. The urea is detected from low to high concentration and the transmission spectrum is recorded sequentially, as shown in Fig. 9(a). The MFI sensing probe is immersed in a certain concentration urea for 20 min. As the urea concentration increases from 0.01 to 100 mM, the wavelength redshift of the MFI sensing probe is an average of 5.13 nm and the first three points are linearly fitted with the sensitivity of 17.29 nm/mM, as shown in Fig. 9(b). Fig. 9(c) shows that two FBGs power difference increases from −5.65 to 18.62 dB and the first three points are linearly fitted with the sensitivity of 81.83 dB/mM. After the MFI has been functionalized, the MFI sensing probe is immersed in DI for 10 min to verify the stability. As shown in Fig. 9(d) and (e), the average standard deviation of the wavelength shift of MFI and two FBGs power difference is 0.043 nm and 0.0551 dB, respectively. The relationship between the wavelength shift and power difference can be expressed by $Y = 4.24X - 5.7$ as shown in Fig. 3(f), which suggests that the wavelength shift of the MFI can be demodulated by the power difference change of two FBGs. The theoretical detection limit of MFI can be calculated as $LOD_1 = 3SD_1/S_1$ [46], where SD_1 is the standard deviation of the error measurements, which is 0.0433 nm, S_1 is the slope

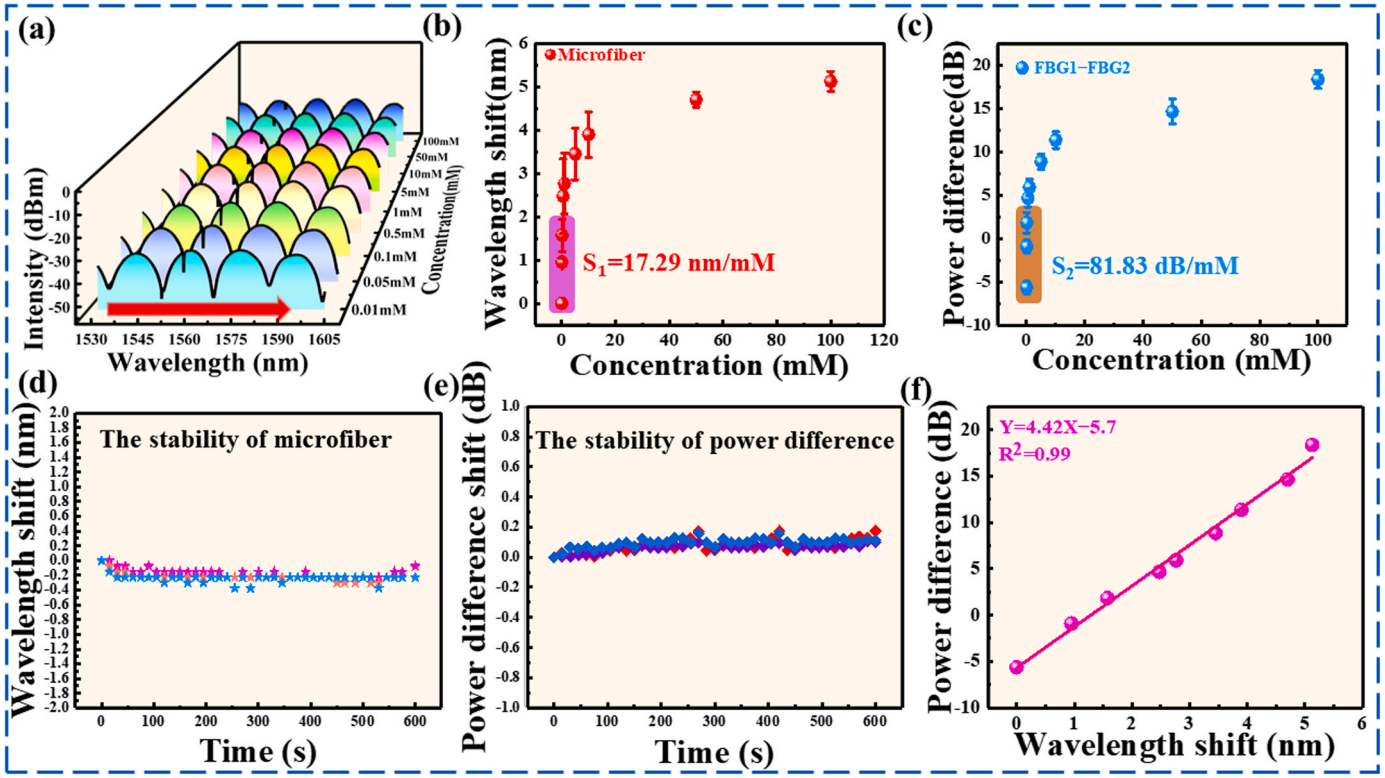

Fig. 9. (a) Transmission spectrum of the differential sensing system for urea in PBS. (b) Response of the MFI sensing probe to urea in PBS. (c) Power difference response of the two FBGs to urea in PBS. (d) Stability of MFI sensing probe in DI for 10 min. (e) Stability of the power difference of two FBGs within 10 min. (f) Relationship between MFI wavelength shift and two FBGs power difference in PBS.

of the fitting curve, which is 17.29 nm/mM, and the LOD_1 can be calculated as 0.007 mM. The same calculation method can be used to obtain the theoretical detection limit of two FBGs power difference, which is $LOD_2 = 3SD_2/S_2$, where $SD_2 = 0.0551$dB, $S_2 = 81.83$dB/mM, and the LOD_2 can be calculated as 0.002 mM. Therefore, based on the experimental results, the differential sensing system can effectively detect urea in PBS. To further characterize the change in orientation of 5CB during urea detection, we perform the same experiment on a slide and observe the light and dark changes of the 5CB appearance during detection of 100 mM urea under POM. The detailed description is shown in Fig. S2 of the Supplementary Material.

3.7. Specific detection

The specificity of the differential sensing system is an essential performance to characterize the sensing performance. The differential sensing system is used to detect different chemical substances with similar structure to urea such as glucose anhydrose, hydroxyurea, thiourea, N,N-Dimethylformamide (DMF), and acetamide. The PBS is selected as the blank control group. First, the different chemical substances are prepared including glucose anhydrous (0.01–100 mM), hydroxyurea (0.01–100 mM), thiourea (0.01–50 mM), DMF (0.01–50 mM), and acetamide (0.01–100 mM). Subsequently, the RI of the chemical substances are measured by the digital refractometer to avoid high RI affecting the experimental results. This detecting process uses the same analytical method used in Section 3.6 for repeating the experiment three times then performing an error analysis and selecting the final stabilized data as the experimental data. As shown in Fig. 10, the wavelength shift and power difference of the differential sensing system for urea, PBS, glucose anhydrous, hydroxyurea, thiourea, DMF, and acetamide are 5.13 nm (22.52 dB), 0.25 nm (0.65 dB), 1.35 nm (5.32 dB), 0.93 nm (5.21 dB), 1.13 nm (5.56 dB), 2.28 nm (9.39 dB), and 1.13 nm (2.28 dB), respectively. It is obvious that the response of the differential sensing system to urea is significantly higher than other chemical substances, which indicates that the sensing system has a good selectivity for urea.

3.8. Urea detection in artificial urine

To demonstrate the practicality of our proposed sensing system, the artificial urine is selected as the relative real environment. Artificial urine main components contained calcium chloride, magnesium chloride, sodium chloride, sodium sulphate, potassium chloride, phosphate, and ammonium chloride. We utilize the differential sensing system to detect the urea in artificial urine with the same concentration as Section 3.6 (0.01–100 mM). Fig. 11(a) shows the transmission spectrum of the differential sensing system to urea in artificial urine. Fig. 11(b) shows that the wavelength redshift of MFI is an average of 2.8 nm as the urea concentration increases from 0.01 to 100 mM and the first three points are linearly fitted with the sensitivity of 3.85 nm/mM. Fig. 11(c) shows that the power difference of the two FBGs increases from −3.84 to 8.67 dB and the first three points are linearly fitted with the sensitivity of 15.05 dB/mM. Fig. 11(d) shows that the linear relationship between the power difference and the MFI wavelength shift can be expressed by $Y = 4.35X - 3.96$. Therefore, the wavelength shift of the MFI can be calculated by obtaining the power difference of two FBGs, which indicates that the OPM can replace the OSA to monitor the urea concentration in artificial urine. The theoretical detection limit of MFI can be calculated as $LOD_3 = 3SD_3/S_3$, where $SD_3 = SD_1 = 0.0433$nm, $S_3 = 3.85$nm/mM and the LOD_3 can be calculated as 0.03 mM. The same calculation method can be used to obtain the theoretical detection limit of two FBGs power difference, which is $LOD_4 = 3SD_4/S_4 = 0.01$ mM, where $SD_4 = SD_2 = 0.0551$dB and $S_4 = 15.05$dB/mM.

Comparing with Section 3.6, the theoretical detection limit of the differential sensing system for urea in PBS is smaller than in artificial urine, which indicates that the impurities in artificial urine interfere with the detection result. Fortunately, due to the specific hydrolysis of urea by urease, the detection limit (0.01 mM) of the differential sensing system in artificial urine is still lower than the normal level range of urea in human urine (0.155–0.39 M). Therefore, it is hoped that the proposed differential sensing system can be applied to the detection of urea in human urine. Table 1 shows the comparison between optical fiber differential sensing system and other detection methods for urea detection. Compared to other detection methods, the differential sensing system combined with MFI and two FBGs has high sensitivity, a low detection limit, and a large detection range and can effectively detect the urea in artificial urine. Furthermore, the use of OPM replaces the OSA to monitor two FBGs intensity changes, which not only optimizes demodulation method but also reduces the cost of the experimental equipment. It is obvious that the differential sensing system is of great significance for urea detection and has applications for the detection of human other disease markers.

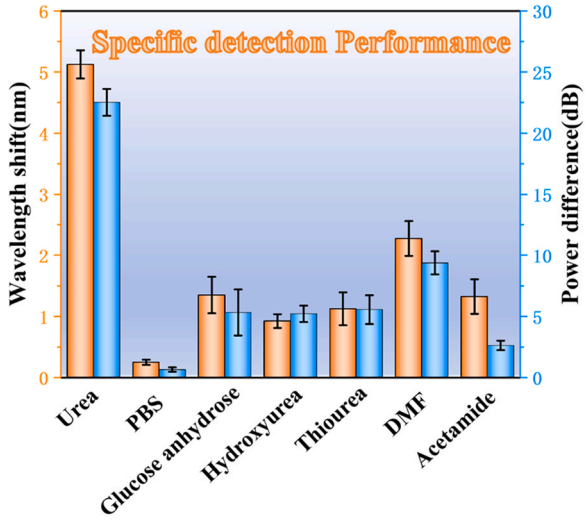

Fig. 10. The specific detection of the differential sensing system.

4. Conclusion

In this paper, an optical fiber differential sensing system based on a cascade of MFI and two FBGs is proposed for urea concentration detection in PBS and artificial urine. The RI sensitivity of the MFI and two FBGs power difference is 1732.24 nm/RIU and 8532.49 dB/RIU, respectively. Furthermore, the RI measurement errors caused by temperature for the MFI is about 2.19×10^{-5} RIU/℃ and the RI measurement errors caused by temperature for the power difference of two FBGs is about 3.86×10^{-5} RIU/℃. The specific recognition molecule urease and the sensitive material SA-doped 5CB are bound to a MFI by covalent bonds. The deprotonation of SA contributed the hydrolysis reaction between urea and urease results in the reorientation of 5CB from planar to homeotropic alignment, which causes the wavelength redshift of the MFI and the change of two FBGs power difference. The experimental results show that the differential sensing system has obvious response to urea in PBS with a detection limit of 0.002 mM in the range of 0.01–0.1 mM. For the urea in artificial urine, the differential sensing system has a detection limit of 0.01 mM in the range of 0.01–0.1 mM, which is well below urea level content in normal human urine. Moreover, there is a good linear relationship between the wavelength shift of the MFI and the power difference variation of two FBGs. On the whole, the proposed differential sensing system has high sensitivity, good specificity, and low temperature cross-sensitivity, which is instructive for the urea detection in artificial urine. In the future, this sensing strategy can be used for the detection of other human disease markers by altering the functional membrane and recognition molecules.

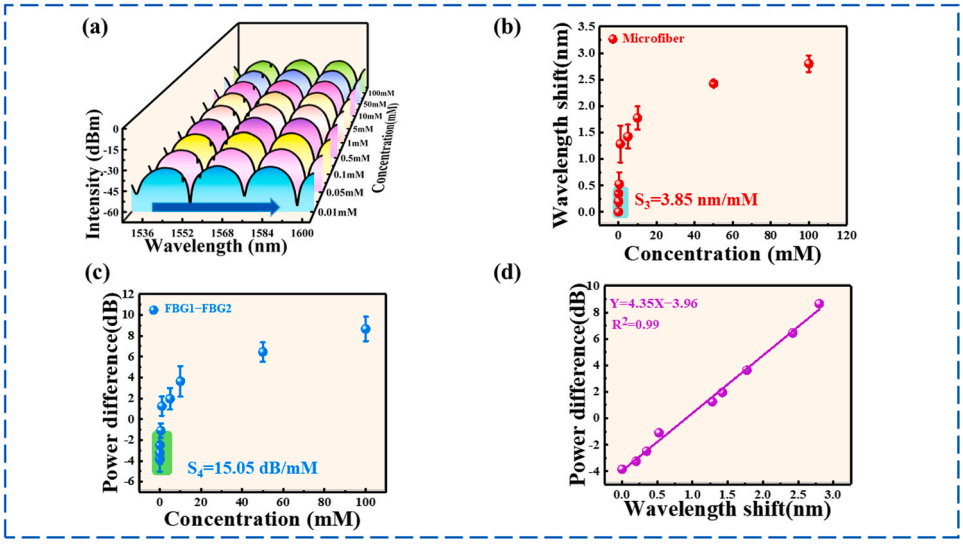

Fig. 11. (a) Transmission spectrum of the differential sensing system to urea in artificial urine. (b) Response of the MFI to urea in artificial urine. (c) Power difference response of two FBGs to urea in artificial urine. (d) Relationship between MFI and two FBGs power difference in artificial urine.

Table 1
Performance comparison of different detection methods for urea detection.

Detection methods	Main chemical materials	Concentration range	Sensitivity	LOD	Manufacturing difficulty	Cost	Refs
A tapered optical fiber	ZIF-8/urease	1–10 mM	0.8 nm/mM	0.1 mM	Easy	Low	[13]
Optical fiber based SPR	Ag/Si/urease	1–160 mM	0.2 nm/mM	-	Difficulty	Low	[12]
Optical fiber based SPR	Ag/ITO/urease entrapped gel	0–160 mM	0.59 nm/mM	0.56 mM	Difficulty	Low	[15]
Optical fiber based SPR	gold film/ ZIF-8/urease	1–7 mM	6 nm/mM	-	Difficulty	Low	[14]
Whisper gallery mode lasing technology based liquid crystal sensor	SA/5CB/urease	0.01–10 mM	-	0.1 mM	Difficulty	High	[25]
Electrochemical	Porous polytetrafluoroethylene/ urease	1.1–20 mM	3.4 mA M^{-1} cm^{-2}	1.1 mM	Difficulty	High	[47]
MFI structure combined with FBG	SA/5CB/urease	0.01–100 mM	3.85 nm/mM (15.05 dB/ mM)	0.03 mM (0.01 mM)	Easy	Low	This work

CRediT authorship contribution statement

Wenwen Wang: Investigation, Data curation. **Jizhou Wu:** Resources, Funding acquisition. **Dandan Sun:** Writing – review & editing, Methodology, Investigation, Funding acquisition. **Jie Ma:** Project administration, Funding acquisition. **Li Jin:** Writing – original draft, Investigation, Data curation. **Bowen Yang:** Formal analysis, Data curation. **Ze Xu:** Investigation, Data curation.

Declaration of Competing Interest

The authors declare that they have no known competing financial interests or personal relationships that could have appeared to influence the work reported in this paper.

Data availability

Data will be made available on request.

Acknowledgments

This work was supported by National Natural Science Foundation of China (62005147, 62175140, U2341211); International Cooperation and Exchange of the National Natural Science Foundation of China (62020106014).

Appendix A. Supporting information

Supplementary data associated with this article can be found in the online version at doi:10.1016/j.snb.2024.136077.

References

[1] K.H. Wang, J.C. Hsieh, C.C. Chen, H.W. Zan, H.F. Meng, S.Y. Kuo, A low-cost, portable and easy-operated salivary urea sensor for point-of-care application, Biosens. Bioelectron. 132 (2019) 352–359.
[2] M. Alqasaimeh, L.Y. Heng, M. Ahmad, A.S. Raj, T.L. Ling, A large response range reflectometric urea biosensor made from silica-gel nanoparticles, Sensors 14 (2014) 13186–13209.
[3] B.K. Boggs, R.L. King, G.G. Botte, Urea electrolysis: direct hydrogen production from urine, Chem. Commun. 32 (2009) 4859–4861.
[4] R. Vanholder, T. Gryp, G. Glorieux, Urea and chronic kidney disease: the comeback of the century?(in uraemia research), Nephrol. Dia. Transpol. 33 (2018) 4–12.
[5] Y. Xie, B. Bowe, T. Li, H. Xian, Y. Yan, Z. Al-Aly, Higher blood urea nitrogen is associated with increased risk of incident diabetes mellitus, Kidney Int. 93 (2018) 741–752.
[6] J. Kawase, H. Ueno, A. Nakae, K. Tsuji, High-performance liquid chromatography of urea and related compounds with post-column derivatization, J. Chromatogr. A 252 (1982) 209–216.
[7] R.Y. Abe, Y. Akutsu, H. Kagemoto, Protein amino acids as markers for biological sources in urban aerosols, Environ. Chem. Lett. 14 (2016) 155–161.
[8] M.K. Reay, C.A. Yates, P.J. Johnes, C.J. Arthur, D.L. Jones, R.P. Evershed, High resolution HPLC-MS confirms overestimation of urea in soil by the diacetyl monoxime (DAM) colorimetric method, Soil Biol. Biochem. 135 (2019) 127–133.
[9] S.S. Mitic, G.Z. Miletic, D.A. Kostic, I.D. Rasic, A spectrophotometric study of streptomycin effect on the clinical urea determination, Chin. J. Chem. 29 (2011) 135–142.
[10] S.K. Wang, C.S.P. Sung, Fluorescence and IR characterization of cure in polyurea, polyurethane, and polyurethane–urea, Macromolecules 35 (2002) 883–888.

[11] S. Singh, M. Sharma, G. Singh, Recent advancements in urea biosensors for biomedical applications, IET Nanobiotechnol. 15 (2021) 358–379.
[12] P. Bhatia, B.D. Gupta, Fabrication and characterization of a surface plasmon resonance based fiber optic urea sensor for biomedical applications, Sens. Actuators B Chem. 161 (2012) 434–438.
[13] G. Zhu, L. Cheng, R. Qi, M. Zhang, J. Zhao, L. Zhu, A metal-organic zeolitic framework with immobilized urease for use in a tapered optical fiber urea biosensor, Microchim. Acta 187 (1) (2020) 9.
[14] L. Cheng, W. Zheng, Y.N. Zhang, X. Li, Y. Zhao, Highly sensitive fiber-optic SPR urea sensor based on ZIF-8/Urease, IEEE Trans. Instrum. Meas. 72 (2023) 1–7.
[15] S. Sharma, S.K. Mishra, Exploiting the advantages of Ag/ITO/Enzyme trapped gel layers to develop a highly sensitive and selective fiber optic plasmonic urea sensor, Chemosensors 11 (2023) 421.
[16] B.O. Guan, Y. Huang, Interface sensitized optical microfiber biosensors, J. Light. Technol. 37 (2018) 2616–2622.
[17] Y. Ran, Z. Xu, M. Chen, W. Wang, Y. Wu, J. Cai, Fiber-optic theranostics (FOT): interstitial fiber-optic needles for cancer sensing and therapy, Adv. Sci. 9 (2022) 2200456.
[18] H.C. Li, Y.K. Leng, Y.C. Liao, B. Liu, W. Luo, J. Liu, Tapered microfiber MZI biosensor for highly sensitive detection of Staphylococcus aureus, IEEE Sens. J. 22 (2022) 5531–5539.
[19] M. Tyagi, A. Chandran, T. Joshi, J. Prakash, V. Agrawal, A. Biradar, Self assembled monolayer based liquid crystal biosensor for free cholesterol detection, Appl. Phys. Lett. 104 (2014) 154104.
[20] R. Duan, Y. Li, Y. He, Y. Yuan, H. Li, Quantitative and sensitive detection of lipase using a liquid crystal microfiber biosensor based on the whispering-gallery mode, Analyst 145 (2020) 7595–7602.
[21] J. Tang, Z. Li, M. Xie, Y. Zhang, W. Long, S. Long, Optical fiber bio-sensor for phospholipase using liquid crystal, Biosens. Bioelectron. 170 (2020) 112547.
[22] J. Hu, D. Fu, C. Xia, S. Long, C. Lu, W. Sun, Fiber Mach–Zehnder-interferometer-based liquid crystal biosensor for detecting enzymatic reactions of penicillinase, Appl. Opt. 58 (2019) 4806–4811.
[23] A. Vahedi, M. Kouhi, Liquid crystal-based surface plasmon resonance biosensor, Plasmonics 15 (2020) 61–71.
[24] D. Liu, C.H. Jang, A new strategy for imaging urease activity using liquid crystal droplet patterns formed on solid surfaces, Sens. Actuators B Chem. 193 (2014) 770–773.
[25] R. Duan, Y. Li, B. Shi, H. Li, J. Yang, Real-time, quantitative and sensitive detection of urea by whispering gallery mode lasing in liquid crystal microdroplet, Talanta 209 (2020) 120513.
[26] G.R. Han, C.H. Jang, Detection of heavy-metal ions using liquid crystal droplet patterns modulated by interaction between negatively charged carboxylate and heavy-metal cations, Talanta 28 (2014) 44–50.
[27] R. Duan, Y. Li, H. Li, J. Yang, Detection of heavy metal ions using whispering gallery mode lasing in functionalized liquid crystal microdroplets, Biomed. Opt. Express 10 (2019) 6073–6083.
[28] X. Bi, D. Hartono, K.L. Yang, Real-time liquid crystal pH sensor for monitoring enzymatic activities of penicillinase, Adv. Funct. Mater. 19 (2009) 3760–3765.
[29] P. Xiao, Z. Xu, D. Hu, L. Liang, L. Sun, J. Li, Efficiently writing Bragg grating in high-birefringence elliptical microfiber for label-free immunosensing with temperature compensation, Adv. Fiber Mater. 3 (2021) 321–330.
[30] C. Zhang, S. Xu, J. Zhao, H. Li, H. Bai, C. Miao, Intensity-modulated refractive index sensor with anti-light source fluctuation based on no-core fiber filter, Opt. Laser Technol. 97 (2017) 358–363.
[31] S.H.K. Yap, Y.H. Chien, R. Tan, A.R. bin Shaik Alauddin, W.B. Ji, S.C. Tjin, An advanced hand-held microfiber-based sensor for ultrasensitive lead ion detection, ACS Sens 3 (2018) 2506–2512.
[32] G. Wang, D. Sun, L. Liang, G. Wang, J. Ma, Highly sensitive detection of trace lead ions concentration based on a functional film-enhanced optical microfiber sensor, Opt. Laser Technol. 161 (2023) 109171.
[33] D. Sun, Y. Fu, Y. Yang, Label-free detection of breast cancer biomarker using silica microfiber interferometry, Opt. Commun. 463 (2020) 125375.
[34] D. Sun, Y. Hao, Y. Fu, J. Ma, Organic dye concentration monitoring through an optical microfiber enabled by multiwalled carbon nanotubes, J. Opt. Soc. B 38 (2021) F178–F185.
[35] L.P. Sun, J. Li, Y. Tan, S. Gao, L. Jin, B.O. Guan, Bending effect on modal interference in a fiber taper and sensitivity enhancement for refractive index measurement, Opt. Express 21 (2013) 26714–26720.
[36] H. Meng, W. Shen, G. Zhang, C. Tan, X. Huang, Fiber Bragg grating-based fiber sensor for simultaneous measurement of refractive index and temperature, Sens. Actuators B Chem. 150 (2010) 226–229.
[37] K. Patel, N. Singh, J. Yadav, J.M. Nayak, S.K. Sahoo, J. Lata, Polydopamine films change their physicochemical and antimicrobial properties with a change in reaction conditions, Phys. Chem. Chem. Phys. 20 (2018) 5744–5755.
[38] N.H. Zainuddin, H.Y. Chee, M.Z. Ahmad, M.A. Mahdi, M.H. Abu Bakar, M. H. Yaacob, Sensitive Leptospira DNA detection using tapered optical fiber sensor, J. Biophotonics 11 (2018) e201700363.
[39] D. Das, S. Sidiq, S.K. Pal, Design of bio-molecular interfaces using liquid crystals demonstrating endotoxin interactions with bacterial cell wall components, RSC Adv. 5 (2015) 66476–66486.
[40] Y.P. Piryatinski, L. Dolgov, O. Yaroshchuk, T. Gavrilko, S. Lazarouk, Enhancement of fluorescence of porous silicon upon saturation by liquid crystal, Opt. Spectrosc. 108 (2010) 70–79.
[41] G. Shen, Y. Guo, X. Sun, X. Wang, Electrochemical aptasensor based on prussian blue-chitosan-glutaraldehyde for the sensitive determination of tetracycline, Nano-Micro Lett. 6 (2014) 143–152.
[42] Y. Wang, Z. Gu, G. Cheng, N. Yuan, J. Ding, Stearic-acid-modified graphene oxide with high dispersion stability and good water-lubricating property, J. Mater. Eng. Perform. (2023) 1–7.
[43] P. Nag, K. Sadani, S. Mohapatra, S. Mukherji, S. Mukherji, Evanescent wave optical fiber sensors using enzymatic hydrolysis on nanostructured polyaniline for detection of β-lactam antibiotics in food and environment, Anal. Chem. 93 (2021) 2299–2308.
[44] S. Jakhar, C. Pundir, Preparation, characterization and application of urease nanoparticles for construction of an improved potentiometric urea biosensor, Biosens. Bioelectron. 100 (2018) 242–250.
[45] T.D.S. Duong, C.H. Jang, Detection of arginase through the optical behaviour of liquid crystals due to the pH-dependent adsorption of stearic acid at the aqueous/liquid crystal interface, Sens. Actuators B Chem. 339 (2021) 129906.
[46] L. Liang, L. Jin, Y. Ran, L.P. Sun, B.O. Guan, Fiber light-coupled optofluidic waveguide (FLOW) immunosensor for highly sensitive detection of p53 protein, Anal. Chem. 90 (2018) 10851–10857.
[47] J.Y. Kim, G.Y. Sung, M. Park, Efficient portable urea biosensor based on urease immobilized membrane for monitoring of physiological fluids, Biomedicines 8 (2020) 596.

Li Jin is currently a postgraduate student in School of Physical and Electronic Engineering, Shanxi University. Her main research interest focues on the optical fiber sensor.

Bowen Yang is currently a postgraduate student in School of Physical and Electronic Engineering, Shanxi University. Her main reaearch focues on the optical fiber sensor.

Ze Xu is currently a postgraduate student in School of Physical and Electronic Engineering, Shanxi University. His main reaearch focues on the optical fiber sensor.

Wenwen Wang is currently a postgraduate student in School of Physical and Electronic Engineering, Shanxi University. His main reaearch focues on optical fiber sensor.

Jizhou Wu received the Ph.D. degree from the Institute of Laser Spectroscopy in Shanxi University, China, in 2012. He has been with the Institute of Laser Spectroscopy, Shanxi University, Taiyuan, China as a Professor since 2021. His research interests are quantum optics, nonlinear optics, optical signal processing technology, and precision measurements.

Dandan Sun received the B.S. degree from Hebei University, Baoding, China, in 2009, the M.S. degree from the Dalian University of Technology, Dalian, China, in 2012, and the Ph. D. degree from the Jinan University, Guangzhou, China, in 2015, respectively. She is currently working as an Associate Professor in School of Physical and Electronic Engineering, Shanxi University, Taiyuan, China. Her research interests focues on the optical fiber sensors and fiber-optic biosensors.

Jie Ma received the B.S. degree and the Ph.D. degree in the department of physics and the Institute of Laser Spectroscopy in Shanxi University, Taiyuan, China, in 2003 and 2009, respectively. He has been with the Institute of Laser Spectroscopy, Shanxi University, Taiyuan, China as a Professor since 2015. His research interests are optical signal processing technology, and ultra-fine measurement systems.